SILICON DOPING PERFORMED BY DIFFERENT DIFFUSION SOURCES AIMING CO-DIFFUSION

Roman Keding, Philip Rothhardt, Christian Roters, Arne Fallisch, Stefan Hohage, Marc Hofmann, Robert Woehl, Dietmar Borchert, Daniel Biro
Fraunhofer Institute for Solar Energy Systems ISE
Heidenhofstraße 2, D-79110 Freiburg, Germany
Phone: +49 761-4588-5197, fax: +49 761-4588-9250
E-Mail: roman.keding@ise.fraunhofer.de

ABSTRACT: In this work several diffusion sources are investigated, aiming at simultaneous phosphorus and boron doping of silicon from different diffusion sources. This challenging process step is called co-diffusion. In the context of this work boron- and phosphorus-doped silicate glass (BSG and PSG) as solid diffusion sources and phosphorus oxychloride ($POCl_3$) as gaseous precursor for phosphorus diffusion are investigated. The combination of solid and gaseous diffusion sources leads to a high flexibility in adjusting sheet resistances on the one hand and to a simplification of process flows on the other. In this work the sheet resistance of p^+-doped areas is varied in the range of $R_{sh} = 50 – 300$ Ω/sq by varying composition and thickness of the solid diffusion sources. The deposition of these solid diffusion sources is carried out by plasma-enhanced chemical vapor deposition (PECVD) using two different process equipments. The excellent passivation capability of the highly p^+-doped silicon surfaces has lead to dark saturation current densities $J_0 = 29.6$ fA/cm^2. In the case of silicon n^+-doping with gaseous diffusion sources, the variation of sheet resistance is possible by adjusting the gaseous composition in the ambience during diffusion. The sheet resistance has been varied in the range of $R_{sh} = 50\text{-}500$ Ω/sq. In the case of n^+-doping the measured dark saturation current densities have been $J_0 = 58.6$ fA/cm^2 and thus show the high potential of these diffusions for implementation in process sequences of high efficiency silicon solar cells.

Keywords: PECVD, Boron, Diffusion, Doping

1 INTRODUCTION

High-efficiency silicon solar cells contain complex doping patterns. These doping patterns consist of p^+- and n^+-doped areas which are generally produced in successive doping processes [1]. If these successive doping processes are performed for the assembly of sophisticated solar cells, process sequences get complex and thus decrease cell throughput. The purpose of this work is the evaluation of a simultaneous diffusion process, which allows n^+- and p^+- doping of silicon in one heat treatment using thermal diffusion from a combination of several solid and gaseous diffusion sources. This process step referred to as co-diffusion leads to a reduction of process steps and hence to a higher throughput. Also an increment of impurity gettering due to simultaneous p^+- and n^+-doping of silicon has already been reported [2].

The effort reduction of process flows due to the implementation of co-diffusion is depicted in Figure 1. In the case of successive diffusion, silicon (1a) is PECVD-coated with silicon oxide (SiO_x) as a diffusion barrier (2a). In (3a) n^+-doping of silicon from phosphorus oxychloride ($POCl_3$) as gaseous phosphorus-precursor is performed. In a chemical two-step reaction the product of $POCl_3$ and oxygen (O_2) reacts with the silicon surface to phosphorus-doped silicate glass ($P+SiO_2$ or PSG). The PSG then works as phosphorus-diffusion source. After the diffusion PSG and SiO_x are wet chemically removed (4a). Subsequently the n^+-doped silicon side is coated with a diffusion barrier (5) and the second diffusion step is carried out using boron bromide (BBr_3) as boron-precursor for p^+-doping (6). Almost similar to the gaseous phosphorus-precursor ($POCl_3$) BBr_3 reacts with O_2 in a two step reaction to boron-doped silicate glass (SiO_2+B, BSG). After diffusion BSG and SiO_x are wet chemical removed (7).

The process sequence of co-diffusion using e.g. one solid and one gaseous diffusion source is less complex. First the silicon wafer (1b) is PECVD-coated with boron-doped silicate glass (SiO_x+B, BSG) (2b). Since the stochiometric composition of PECVD layers is in general incorrect, we have to write SiO_x instead of SiO_2. Immediately after the $POCl_3$-diffusion step, the simultaneous diffusion of the p^+-doped area from BSG and the n^+-doped area from $POCl_3$ is performed (3b). After diffusion PSG and BSG are wet chemically removed (4b).

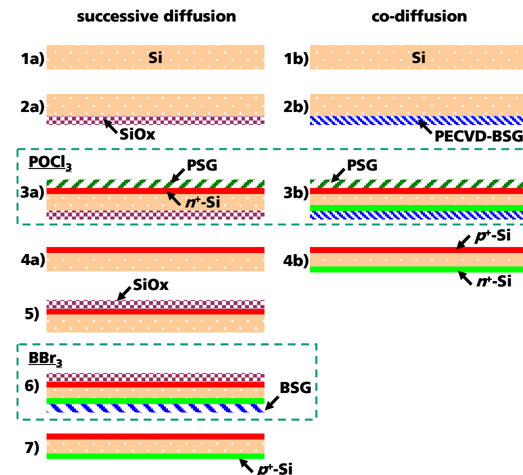

Figure 1: Process sequence of successive (left side) and co-diffusion (right side). The comparison of both process sequences shows the reduced number of process steps of a co-diffusion treatment compared to a successive one.

The comparison of the successive and the co-diffusion process flow shows the reduction in process effort using co-diffusion processes for silicon doping. $POCl_3$ and BBr_3 as gaseous diffusion precursors as well as PSG and BSG as solid diffusion sources can be exchanged with each other. In the framework of this

work co-diffusion with the combination of solid BSG, PSG and gaseous $POCl_3$ are mainly in focus. Therefore, diffusion sources are investigated separately using the same temperature conditions during diffusion for each process.

2 INVESTIGATION OF THE BSG-PROCESS

2.1 Process setup and sample preparation

The deposition of BSG is done in an inline PECVD system (SINA, Roth and Rau). As reactant gases, nitrous oxide (N_2O), silane (SiH_4), argon (Ar), and diborane (B_2H_6) as boron donator are used for the deposition of BSG. The plasma excitation is carried out with the energy of pulsed microwaves (MW) coupled into with a linear antenna.

For further characterization of the standard BSG-process symmetrical lifetime samples were prepared. These samples allow the evaluation of the sheet resistance and the concentration profiles on the one hand and also offer the extraction of dark saturation current densities on the other hand, if passivated. For the fabrication of these samples FZ (float zone) silicon material with smooth surfaces and a *p*-type base doping was used. After BSG deposition on both sides of the wafers, the wafers were diffused in a tube furnace.

In a first experiment the thermal budget of diffusion was fixed for regarding the influence of BSG on diffusion due to thickness and boron concentration. Therefore a maximal temperature $T_M = 950°C$ and a plateau time $t_p = 30$ min were selected for diffusion. For evaluating the influence of BSG-film thickness on boron diffusion into silicon, the thickness was varied in the range $50 < h_{BSG} < 300$ nm. The boron concentration of the deposited layers was adjusted by the gas flow ratio of diborane to silane $r = Q_{B2H5} / Q_{SiH4}$. Here a ratio of $r = 33.3$ % was used, which is the maximum value reachable within the PECVD-setup. For evaluating the influence of the boron concentration on diffusion, the BSG-film thickness was fixed at $h = 200$ nm and the gas flow ratio varied in the range $13.3 < r < 33.3$ %. Within the first experiment *p*-type substrates with a specific base resistivity $\rho = 0.5$ Ωcm were used.

In a second experiment the thermal budget during diffusion was varied. In order to get a hint of the temperature and time impact on boron diffusion from BSG, two diffusion maximal temperatures of $T_M = 950°C$ and 1050°C as well as two diffusion plateau times $t_p = 30$ min and 60 min were combined with each other leading to four different temperature budgets. The boron diffusion was carried out from BSG-layers with high boron concentration and high BSG-thickness. The symmetrical diffused samples from the second experiment were PECVD-coated with a passivation stack consisting of aluminum oxide (AlO_x) and silicon nitride (SiN_x) on both sides, and measured with quasi steady state photoconductance (QSSPC) after a forming gas anneal (FGA). Within the second experiment *p*-Type substrates with a specific base resistivity $\rho = 1$ Ωcm were used.

2.2 Influence of BSG composition on boron diffusion

In Figure 2 the dependence of sheet resistance R_{sh} on BSG-film thickness h_{BSG} is shown. The sheet resistance decreases with increasing film thickness and saturates for film thicknesses of BSG higher than $h_{BSG} > 200$ nm. To investigate the influence of the timeframe between BSG deposition and boron diffusion from BSG, some samples were diffused two weeks after deposition. As depicted in Figure 2, starting diffusion directly after BSG deposition and two weeks later provides the same results. Thus, BSG does not degrade in ambient air.

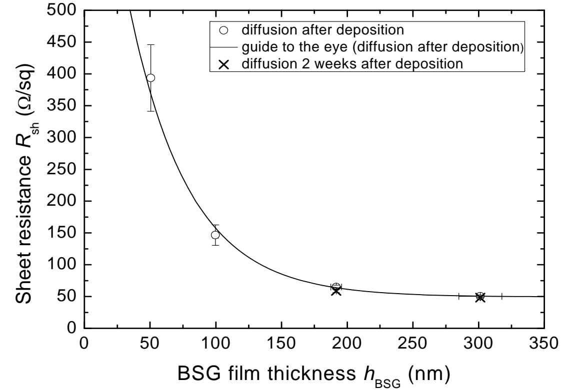

Figure 2: Sheet resistance of p^+-doped area diffused from BSG as a function of BSG-film thickness h_{BSG}. Sheet resistance decreases for higher BSG-thicknesses and saturates for $h_{BSG} > 200$ nm. The error bar indicates the standard deviation of R_{sh}-mean values upon three wafer samples.

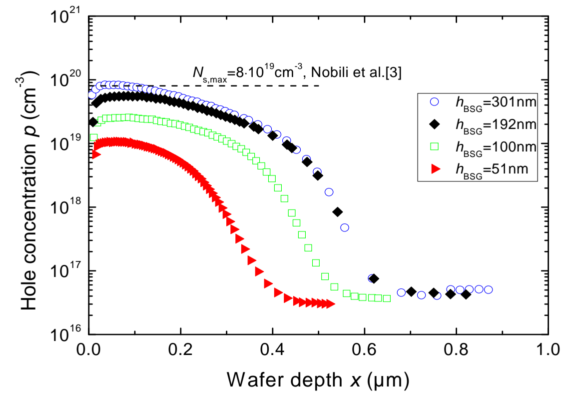

Figure 3: Hole concentration *p* in dependence on wafer depth *x* measured with ECV on the p^+-doped areas diffused from BSG. By varying the BSG-film thickness h_{BSG} differences in the hole concentration are caused.

In Figure 3 the concentration profiles measured by electrochemical capacitance voltage (ECV) measurements corresponding to the sheet resistances in Figure 2 are shown. Since ECV measures the effective carrier concentration, here the hole concentration *p* is plotted against wafer depth *x*. Assuming only active boron atoms in silicon, the hole concentration almost equals the acceptor concentration N_A and thus the boron concentration N_B in silicon. The maximal boron concentration of $N_{B,max}$ as well as the depth x_{pn} of profiles shrinks for thinner BSG-layers. Using a BSG-layer with a thickness of approximately 300nm leads to an p^+-doped area with a maximal boron concentration $N_{B,max} = 8 \cdot 10^{19}$ cm^{-3}. This high concentration value corresponds to the maximum boron concentration $N_{s,max}$ reachable for $T = 950°C$ according to Nobili et al.[3]. The depth of the concentration profiles is only dependent on thickness for thin layers $h_{BSG} < 200$ nm. This effect is probably due to the finite character of thin diffusion

sources. Nevertheless, diffusion profiles with a depth deeper than 0.6 µm are reached by using BSG-layers with a thickness higher than 200 nm.

In Figure 4 the dependence of sheet resistance on boron concentration is presented. The boron concentration in BSG is expressed by the gas flow ratio r of Q_{B2H6} to Q_{SiH4}. With an increasing r the sheet resistance decreases and saturates beyond a certain value. This is due to the fact that the maximum solubility and diffusion length of boron in silicon depends on temperature conditions during diffusion [4]. Thus the sheet resistance has also a lower limit which depends on temperature conditions. Here, trusting the exponential guide to the eye fitted with the actual experimental data, this lower limit would be in the range of $50 < R_{sh} < 55$ Ω/sq. This fact would also correspond to the results shown in Figure 2. An R_{sh}-value measured in an earlier experiment matches the guide to the eye and can thus be understood as an indication for process reproducibility.

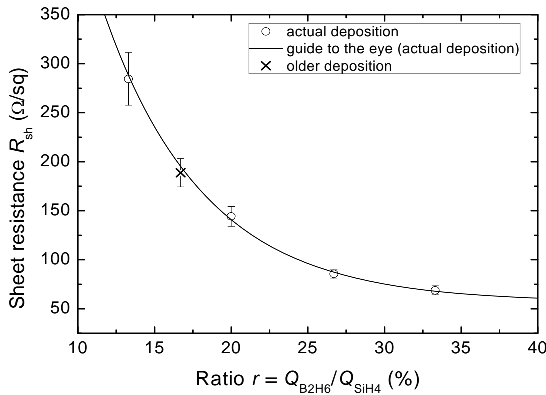

Figure 4: Sheet resistance of p^+-doped areas diffused from BSG as a function of gas flow ratio r. This ratio refers to the boron concentration in BSG. The sheet resistance decrease exponentially with increasing ratios. The error bar indicates the standard deviation of R_{sh}-mean values upon 3 wafer samples.

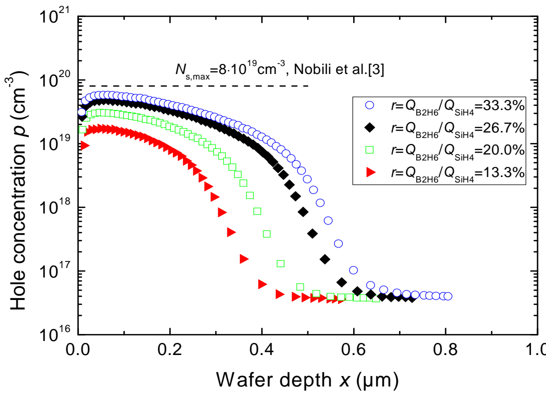

Figure 5: Hole concentration p in dependence on wafer depth x measured by ECV on the p^+-doped areas diffused from BSG. By varying the flow ratio r of Q_{B2H6} and Q_{SiH4} while depositing BSG the profiles differ from each other in depth and maximal hole concentration.

In Figure 5 the ECV-data corresponding to the R_{sh}-values in Figure 4 is presented. As is shown, the maximum boron concentration $N_{B,max}$ as well as the profile depth x_{pn} decreases with decreasing gas flow ratios r. This is due to the fact that the diffusion sources with lower boron concentration get finite after shorter diffusion times, compared to the sources with higher boron concentration. After a certain time, boron concentration in silicon decreases and thus also the diffusivity of boron in silicon, which depends on boron concentration in silicon itself [5]. The diffusivity loss of boron in silicon due to smaller boron concentration leads to shallower concentration profiles.

2.3 Influence of thermal budget during boron diffusion

By means of ECV-profiles, the influence of diffusion plateau time t_p and maximal temperature T_M on boron diffusion from BSG is depicted in Figure 6. The sheet resistances R_{sh} corresponding to the profiles were calculated with the following formula

$$R_{sh} = \frac{1}{\int \sigma \, dx} \approx \frac{1}{q \int_0^{x_{pn}} p(x)\mu_p(p)\,dx}$$

where σ is the conductivity, x is the wafer depth, q is the elementary charge and μ_p is the hole mobility in silicon. The hole mobility in dependence on hole concentration $\mu_p(p)$ was calculated using the mobility model after Klaassen et al.[6]. The calculated sheet resistances are listed in Table I. An increasing temperature budget during diffusion leads to a reduction of sheet resistance. In the case of $T_M = 950$°C, the maximum boron concentration $N_{B,max}$ equals the maximal boron solubility in silicon $N_{s,max}$ ($T_M = 950$°C) $= 8\cdot10^{19}$ cm^{-3} for short and long diffusion times. Thus, the diffusion source has an infinite character during the whole diffusion time span from 30 to 60min.

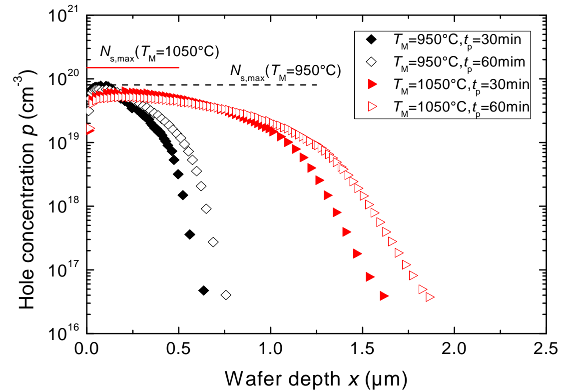

Figure 6: Hole concentration p in dependence on wafer depth x measured by ECV. The shape differences of the several profiles can be reached by varying the temperature budget during thermal treatment. The $N_{s,max}$-values (boron solubility of boron in silicon) are according to Nobili et al [3].

In the case of a maximal temperature $T_M = 1050$°C, the maximal boron concentration is $N_{B,max} = 5\text{-}6\cdot10^{19}$ cm^{-3} and thus one order of magnitude smaller than the maximum solubility of boron $N_{s,max} = 1.5\cdot10^{21}$ cm^{-3} but also smaller than the $N_{B,max}$-value of the diffusion carried out with a maximal temperature $T_M = 950$°C. Hence, the diffusion source is certainly finite for $T_M = 1050$°C in the regarded time range. Infinite diffusion sources for maximal temperatures $T_M = 1050$°C can be reached by thickening the BSG-layers or increasing the boron concentration in BSG. The strong dependence of diffusion depth on temperature, compared to the

influence of diffusion time is clearly visible. Performing boron diffusion from BSG with a maximal temperature of T_M = 1050°C leads to a diffusion depth approximately 2.5 times deeper compared to T_M = 950°C.

Table I: Extracted values from the concentration profiles in Figure 6. The depth x_{pn} was extracted at $p = 10^{17}$ cm^{-3}. $R_{sh,C}$ refers to the calculated sheet resistance using the ECV-profiles.

T_M (°C)	t_p (min)	$R_{sh,C}$ (Ω/sq)	$N_{B,max}$ (cm^{-3})	x_{pn} (µm)
950	30	69.9	7.7 10^{19}	0.61
950	60	52.7	6.8 10^{19}	0.72
1050	30	24.7	6.1 10^{19}	1.51
1050	60	24.5	5.2 10^{19}	1.75

In Figure 7 the measured effective lifetime τ_{eff} in dependence on excess carrier density Δn measured with QSSPC at room temperature (RT = 298K) is presented. The saturation current density J_0 was determined under low injection ($\Delta n \leq 0.1 \cdot N_A$) at $\Delta n = 10^{15}$ cm^{-3}.

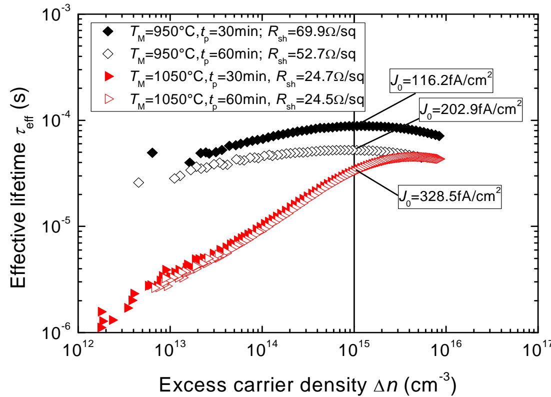

Figure 7: Effective lifetime τ_{eff} in dependence on excess carrier density Δn. The $p^+/p/p^+$-samples are passivated by a PECVD AlO_x/SiN_x Stack. The J_0-values are determined at $\Delta n = 10^{15}$ cm^{-3} (low injection, $N_A = 1.5 \cdot 10^{16}$ cm^{-3}) and $T=RT$ ($n_i = 9.1 \cdot 10^9$ cm^{-3}).

For increasing temperature budgets during diffusion which correspond to decreasing sheet resistances the saturation current density increases. This effect is probably caused by an increase of auger recombination due to the higher doping-levels reached at higher diffusion budgets. Also remarkable is the strongly decreased effective lifetime under very low injection levels for high diffusion budgets, which might be caused by an increased Shockley-Read-Hall (SRH) recombination in the bulk.

3 ALTERNATIVE BSG-PROCESS

3.1 Process setup and sample preparation

The second BSG-deposition process is carried out with a prototype PECVD-equipment of Centrotherm. The energy for plasma activation is induced by a high frequency AC-voltage (rf = 13.56 MHz). The electrode arrangement is symmetrical capacitive. For the deposition of BSG diborane (B_2H_6), silane (SiH_4) and nitrous oxide (N_2O) have been used.

For evaluation of sheet resistance, concentration profile as well as dark saturation current densities, again symmetrical lifetime samples were prepared. After optimization of process parameters like e.g. process pressure, process gas flows were varied aiming at higher boron concentration in BSG. Hence, a variation of the silane gas flow Q_{SiH4} has lead to a significant impact on function ability of BSG as diffusion source. The deposition time was adjusted aiming at a BSG-film thickness of h_{BSG} = 200nm. The samples were made on FZ-silicon p-type material with a base resistivity ρ = 10 Ωcm. After diffusion (T_M = 950°C, t_p = 30 min) the samples were coated with a stack consisting of ALD-AlO_x (ALD, atomic layer deposition) and PECVD-SiN_x. Finally, for activation of passivation quality a FGA was performed.

3.2 Results of silane gas flow variation

In Figure 8 the strong dependence of sheet resistance R_{sh} on silane gas flow Q_{SiH4} during BSG deposition is presented.

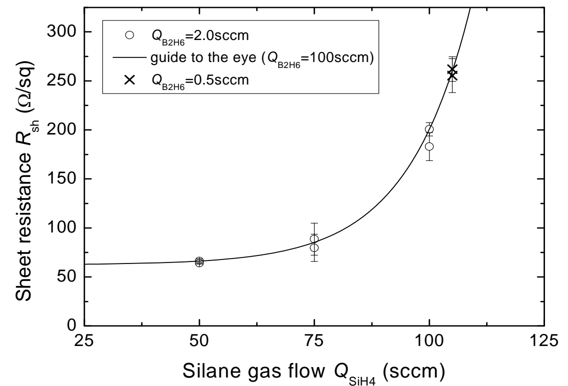

Figure 8: Sheet resistance of p^+-doped areas diffused from BSG as a function of the silane gas flow Q_{SiH4} and diborane gas flow Q_{B2H6}. The error bar indicates the standard deviation of R_{sh}-mean values upon three wafer samples.

For a decreasing silane gas flow the sheet resistance decreases until saturation occurs. The measurement data has been fitted exponentially by just using the R_{sh}-values realized from BSG, deposited with a high diborane gas flow Q_{B2H6} = 2 sccm. To investigate the sheet resistance dependency on the diborane gas flow, also a lower gas flow (Q_{B2H6} = 0.5 sccm) was used during BSG-deposition. Trusting the guide to the eye, Q_{B2H6} has no significant impact on boron diffusion from BSG. The gas flow ratio of r = 4 % (Q_{B2H6} = 2 sccm, Q_{SiH4} = 50 sccm) is the highest one reachable within the PECVD-setup and leads to a sheet resistance R_{sh} = 64.0 ± 0.9 Ω/sq.

In Figure 9 the ECV-measured concentration profiles of process 1 (rf-source) and former process 2 (MW-source) are compared. Both were diffused from BSG sources with a thickness of about h_{BSG} = 200 nm and the maximum boron concentration reachable within the PECVD-setups. It is clearly visible that the maximum boron concentration $N_{B,max}$, and the depth x_{pn} are almost the same. The calculated sheet resistances $R_{sh,C}$ from the profiles correspond to the measured ones $R_{sh,M}$. This can be accepted as a verification of the ECV-measurements. The characterizing values of each profile are summarized in Table II.

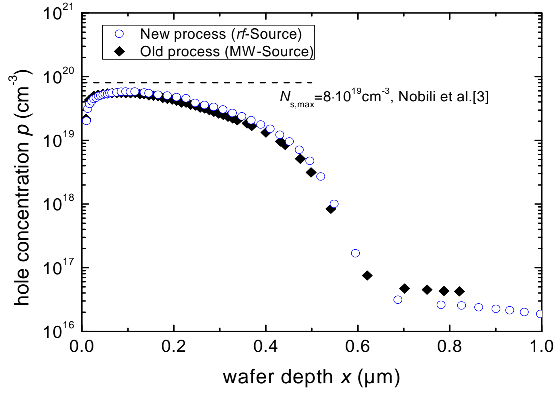

Figure 9: Comparison of the ECV-measured concentration profiles diffused from BSG deposited with two different PECVD setups.

Table II: Extracted values from the concentration profiles in Figure 9. Depth x_{pn} was extracted at $p = 10^{17}$ cm^{-3}.

Process (-)	$R_{sh,M}$ **(Ω/sq)**	$R_{sh,C}$ **(Ω/sq)**	$N_{B,max}$ **(cm^{-3})**	x_{pn} **(µm)**
rf-source	64.0±0.9	63.8	$5.83\ 10^{19}$	0.63
MW-source	65.8±5.9	69.0	$5.55\ 10^{19}$	0.61

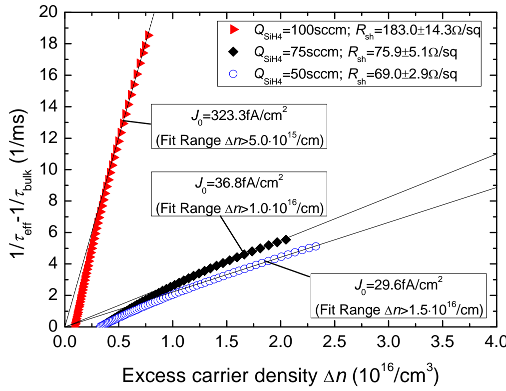

Figure 10: Inverse bulk-corrected lifetime $1/\tau_{eff} - 1/\tau_{bulk}$ measured with QSSPC as a function of excess carrier density Δn. The saturation current densities have been determined using the slope method under high injection conditions ($N_A = 1.5\cdot10^{15}$ cm^{-3}, $T = RT$, $n_i = 8.5\cdot10^{9}$ cm^{-3}).

In Figure 10 the bulk corrected effective lifetime $1/\tau_{eff} - 1/\tau_{bulk}$ measured by QSSPC is plotted over the excess carrier density Δn. By using the slope method [7], dark saturation current densities J_0 can be determined from the data under high-injection conditions. In Figure 10, the calculated J_0-values are also inserted. As can be seen, very low J_0-values below 30 fA/cm^2 were realized due to low recombination in the p^+-doped areas and an excellent surface passivation of the silicon surface by ALD-AlO_x. Interesting is the theoretical unexpected increase of recombination for increasing sheet resistances R_{sh}, as realized from BSG deposited with high silane gas flows Q_{SiH4}. This increase in J_0 as well as the hydrophilic character of these samples after diffusion and BSG removal can be taken as an indication that boron residuals like silicon borides are situated at the silicon surface and thus decrease the silicon surface passivation ability. This influence of PECVD on the formation of silicon borides will be investigated in further studies.

4 IMPROVEMENT OF PHOSPHORUS DIFFUSION

4.1 Process setup and sample preparation

The adjustment of sheet resistance by varying the composition of the gaseous mixture during heat treatment has been investigated by Rothhardt et al.[8] and will also be published at this conference. The diffusion has been carried out in a tube furnace (Centrotherm). The gaseous mixture includes phosphorus oxychloride ($POCl_3$), oxygen (O_2) and nitrogen (N_2). In this work, one diffusion scheme has been implemented in symmetrical lifetime samples, aiming at low recombination losses. The temperature budget during heat treatment corresponds to the temperature budget used for boron diffusion ($T_M = 950$°C, $t_p = 30$min). Some samples were also coated with PECVD-PSG/SiO_x stacks as proposed by Fallisch et al.[9] and diffused in the same heat treatment as well.

The symmetrical lifetime samples were prepared on textured FZ-material with a *p*-type base doping ($\rho = 1\Omega$cm). After diffusion the samples were coated with a front side passivation stack, consisting of a thin silicon rich siliconoxynitride ($SiON_x$) and a silicon nitride (SiN_x) anti-reflection coating on top of it [10]. After passivation a FGA was performed.

4.2 Results of phosphorus diffusion from phosphorus diffusion sources

In Table III the sheet resistance R_{sh}, maximum phosphorus concentration $N_{P,max}$ and depth x_{pn} of the n^+-doped areas realized with several process options are summarized. In the case of process P1 to P4 $POCl_3$ has been used as phosphorus-precursor for phosphorus diffusion, whereas the composition of gaseous mixture during heat-treatment has been varied. In the case of process P5 PSG has been used as diffusion source.

Table III: Extracted values of the different n^+-doped areas. Depth x_{pn} and $N_{P,max}$ were measured with ECV. Depth x_{pn} was extracted at $n = 10^{17}$ cm^{-3}.

Process (-)	**Surface (-)**	R_{sh} **(Ω/sq)**	$N_{P,max}$ **(cm^{-3})**	x_{pn} **(µm)**
$POCl_3$,P1	smooth	48.7±2.7		
$POCl_3$,P2	smooth	133.0±2.8	$4.0\cdot10^{19}$	0,36
$POCl_3$,P3	smooth	157.2±2.8	$3.3\cdot10^{19}$	0,33
$POCl_3$,P3*	textured	243.9±15.9		
$POCl_3$, P4	smooth	259.6±11.9	$2.2\cdot10^{19}$	0,28
PSG, P5	smooth	30.7±3.0	$2.3\cdot10^{20}$	0.68

*QSSPC-samples

The R_{sh}-values can be adjusted in a wide range. Also remarkable is the strong influence of surface topography on phosphorus diffusion. By using an alkaline textured wafer (P3*) surface instead of a smooth surface (P3) leads to an R_{sh}-increase of approximately $\Delta R_{sh} = 55$ %. Hence, phosphorus diffusion is strongly weakened by textured surfaces. The ECV-profiles of the n^+-areas diffused from $POCl_3$ (P3) and PSG (P5) are depicted in Figure 11. Compared to the n^+-areas diffused from PSG, the one diffused from $POCl_3$ is quite shallow and has a lower phosphorus surface concentration. The value of the

dark saturation current density measured on a textured (P3*) symmetrical life time sample is included as well. Due to the low phosphorus concentration in the n^+-silicon on the one hand as well as adequate silicon surface passivation by $SiON_x$ on the other dark saturation current densities $J_0 < 60$ fA/cm² can be reached.

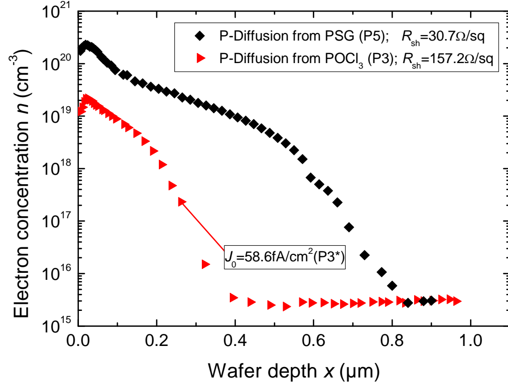

Figure 11: ECV-profile of n^+-doped areas diffused from $POCl_3$ (process 3) and from PSG. The J_0-value corresponding to the $POCl_3$-process has been determined from textured (process 3*) $n^+/p/n^+$-samples passivated by a PECVD $SiON_x$/AR-SiN_x Stack (low injection, $\Delta n = 1 \cdot 10^{15}$ cm^{-3}, N_A=1.5*10^{16} cm^{-3}, n_i=9.1·10^9 cm^{-3}).

5 CONCLUSION AND OUTLOOK

It could be shown that diffusion from solid diffusion sources like BSG and PSG as well as diffusion from gaseous phosphorus-precursor like $POCl_3$ result in suitable R_{sh}-values for solar cell processing. Thereby all the diffusion processes were carried out in one thermal process with constant temperature budget (T_M = 950°C, t_p = 30 min). Hence the combination of the several diffusion processes for co-diffusion purposes is possible.

Also passivation capability of the diffused silicon surfaces after boron and phosphorus diffusion could be proved. In the case of boron diffusion from BSG very low dark saturation current densities of J_0=29.6 fA/cm² could be achieved on highly p^+-doped areas (R_{sh} = 63.8 Ω/sq, $N_{B,max}$=5.83·10^{19} cm^{-3}) by using a passivation stack consisting of ALD AlO_x and PECVD SiN_x. In the case of phosphorus diffusion from $POCl_3$ dark saturation current densities J_0=58.6 fA/cm² were achieved on textured, n^+-doped surfaces (R_{sh} = 243.9 ± 15.9 Ω/sq, $N_{P,max} \leq$ 3.3·10^{19} cm^{-3}) using a passivation stack consisting of PECVD $SiON_x$ and AR-SiN_x. The limitation in open-circuit voltage due to recombination in the highly doped regions and at the silicon surfaces can be calculated [11]. For a back-contact back-junction solar cell (Emitter fraction = 80 %) this limitation would be $V_{OC,limit}$ = 685 mV. For a PERC-cell structure without selectively doped areas this limitation would be $V_{OC,limit}$ = 690 mV. These high values certainly show the feasibility of the diffusion processes also for sophisticated high efficiency silicon solar cells.

Since within this work all the diffusions from the different sources were carried out separately, further investigations will focus on the challenging diffusion from all sources in one heat treatment.

6 ACKNOWLEDGEMENTS

This work was supported by the European Union - European Fond for regional development "Investments for the Future" and the government of Northrhine-Westphalia under contract number 64.65.69-EN-2001A (ALPS)".
The technical assistance of R. Neubauer and D. Trogus is greatly acknowledged.

7 REFERENCES

[1] F. Granek, M. Hermle, C. Reichel, O. Schultz-Wittmann, and S. W. Glunz, "High- efficiency back-contact back-junction silicon solar cell research at Fraunhofer ISE," presented at Proceedings of the 23rd European Photovoltaic Solar Energy Conference, Valencia, Spain, 2008.

[2] J. Schön, M. C. Schubert, W. Warta, H. Savin, and A. Haarahiltunen, "Analysis of simultaneous boron and phosphorus diffusion gettering in silicon," *Physica Status Solidi A*, vol. 207, pp. 2589–92, 2010.

[3] D. Nobili, "Solubility of boron in silicon," *Properties of Silicon*, p. 394, 1987.

[4] P. Y. Yu and M. Cardona, *Fundamentals of Semiconductors*, 2nd edition ed. Berlin, Heidelberg, New York: Springer, 2003.

[5] O. V. Aleksandrov, "Simulation of the concentration dependence of boron diffusion in silicon," *Semiconductors*, vol. 38, pp. 258-261, 2004.

[6] D. B. M. Klaassen, "A unified mobility model for device simulation - I. Model equations and concentration dependence," *Solid-State Electronics*, vol. 35, pp. 953-9, 1992.

[7] A. Cuevas and D. Macdonald, "Measuring and interpreting the lifetime of silicon wafers," *Solar Energy*, vol. 76, pp. 255-62, 2004.

[8] N. Mingirulli, R. Keding, J. Specht, A. Fallisch, D. Stüwe, and D. Biro, "Hot-melt inkjet as masking technology for back-contacted cells," presented at Proceedings of the 34th IEEE Photovoltaic Specialists Conference, Philadelphia, 2009.

[9] A. Fallisch, D. Wagenmann, R .Keding, D. Trogus, M. Hofmann; J. Rentsch; H. Reinecke and D.Biro, "Analysis of Phosphorus-Doped Silicon Oxide Layers Deposited by Means of PECVD as a Dopant Source in Diffusion Processes," *IEEE Journal of Photovoltaics*, vol.PP, no.99, pp.1-7, 0 doi: 10.1109/JPHOTOV.2012.2200455

[10]J. Seiffe, L. Gautero, M. Hofmann, J. Rentsch, R. Preu, S. Weber, and R. A. Eichel, "Surface passivation of crystalline silicon by plasma-enhanced chemical vapor deposition double layers of silicon-rich silicon oxynitride and silicon nitride," *Journal of Applied Physics*, vol. 109, pp. 034105, 2011.

[11]S. Kluska, F. Granek, M. Hermle, and S. W. Glunz, "Loss analysis of high-efficiency back-contact back-junction silicon solar cells," presented at Proceedings of the 23rd European Photovoltaic Solar Energy Conference, Valencia, Spain, 2008.